Au_{40}: A large tetrahedral magic cluster

De-en Jiang and Michael Walter

Phys. Rev. B **84**, 193402 — Published 8 November 2011

DOI: 10.1103/PhysRevB.84.193402

Au_{40}: A Large Tetrahedral Magic Cluster

De-en Jiang[1] and Michael Walter[2]
[1] *Chemical Sciences Division, Oak Ridge National Laboratory, Oak Ridge, TN 37831-6201 and*
[2] *Freiburg Materials Research Center, Stefan-Meier-Str. 21, 79104 Freiburg, Germany*

40 is a magic number for tetrahedral symmetry predicted in both nuclear physics and the electronic jellium model. We show that Au_{40} could be such a a magic cluster from density functional theory-based basin hopping for global minimization. The putative global minimum found for Au_{40} has a twisted pyramid structure, reminiscent of the famous tetrahedral Au_{20}, and a sizable HOMO-LUMO gap of 0.69 eV, indicating its molecular nature. Analysis of the electronic states reveals that the gap is related to shell closings of the metallic electrons in a tetrahedrally distorted effective potential.

PACS numbers: 61.46.Bc, 36.40.Cg, 31.15.E-

Gold is a magic element that constantly brings us surprises. The relativistic effect has been demonstrated to be a dominating factor that distinguishes gold from the same-group elements such as copper and silver[1]. Many intriguing structures and properties are found for nanometer-sized gold clusters. One example is the transition from a two-dimensional structure to a three-dimensional one around a size of 10 atoms[2,3]. Another is the unique catalytic activity of nanometer-sized gold clusters[4].

Among all gold nanoclusters, Au_{20} is probably the most famous one[5]. It has a simple tetrahedral symmetry with every gold atom on the surface. The tetrahedral symmetry is very stable and is the ground state both in charged and neutral clusters[6]. The symmetry is still retained if one atom is removed to form Au_{19}[6] and is proposed to be present in chemically synthesized $Au_{20}(PPh_3)_8$ clusters[7].

It is common for gold clusters that the frontier orbitals around Fermi energy are derived from Au($6s$) atomic orbitals and form delocalized states distributed over the whole cluster[8]. Very similar to the stability of noble gas atoms in the periodic system of elements, a closed electronic shell built up from these delocalized states improves the energetics and gives more chemical stability, i.e. reduced reactivity[9]. This effect also leads to enhanced stability for specific sizes in protected gold clusters[10,11]. Spherical shell closings are especially prominent as these are known to lead to large gaps between highest occupied (HOMO) and lowest unoccupied molecular orbitals (LUMO), the signature of chemical stability.

In the case of deformations of the background potential, the Jahn-Teller effect can lead to stabilizations where spherical shell closings are not available[9]. A special case here is octupole deformations, where in particular tetrahedral deformations produce large gaps[12].

The appearance of tetrahedral deformations is proposed in nuclear physics[13] where the delocalized particle picture in an effective background potential had originated before it was adopted in cluster physics. While the experimental observation of the tetrahedral deformation in nuclei seems to be under debate[14,15], the importance of tetrahedral symmetry in cluster physics in the case of Au_{20} is beyond question[16].

Magic tetrahedral metal clusters were proposed in the jellium model[12]. In particular, in the essentially parameter-free ultimate jellium model, where the smeared out nuclear density exactly follows the electronic density, the 40 electron ground state shows a tetrahedral deformation[17]. In spherical symmetry the electrons' angular momentum is conserved and the relative energies of different angular momentum shells (and also the gaps between them) depend on the effective radial potential. There is a large gap for a harmonic radial potential at 40 electrons. This gap decreases when the potential becomes more box like, however[9]. Here a tetrahedral deformation can open the gap again. To our knowledge, tetrahedral metal clusters larger than the rather trivial case of four atoms have been observed only in the example of Au_{20}. In this Letter, we show from density functional theory-based global minimization that the larger Au_{40} has a twisted trigonal pyramid structure of quasi-tetrahedral symmetry, the first case of a metal cluster of tetrahedral shape beyond Au_{20}.

Although gold clusters with 20 atoms or less have been extensively studied, we know relatively little of the structures of larger gold clusters. Au clusters with 30 to 60 atoms would be the key to understanding the transition from the molecular behavior of a small cluster to the metallic bulk. The clusters Au_{32}[18,19] and Au_{34}[20] have been proposed to have a core-shell structure, instead of being hollow or planar. More recently, the global minima of Au_{28} to Au_{35} were explored in comparison with experimental photoelectron spectra[21]. The authors found that the global minima are amorphous in nature with an Au_4 tetrahedron core and a much bigger outer-shell for Au_N with $N > 32$. Using an empirical potential for global minimum search followed by density functional theory (DFT) calculations, Garzón et al. found that the most stable structure of Au_{38} is of C_s symmetry with an Au_5 core[22,23]. This structure was found to be slightly lower in energy than the high-symmetry truncated octahedron (by about 0.3 to 0.6 eV, depending on the choice of DFT functional[22,23]). Both the C_s and octahedral structures are metallic (that is, their HOMOs are not completely

filled). Using a strategy similar to Garzón et al.'s, Tran and Johnston found a structure for Au_{40} with a distorted truncated octahedron[24].

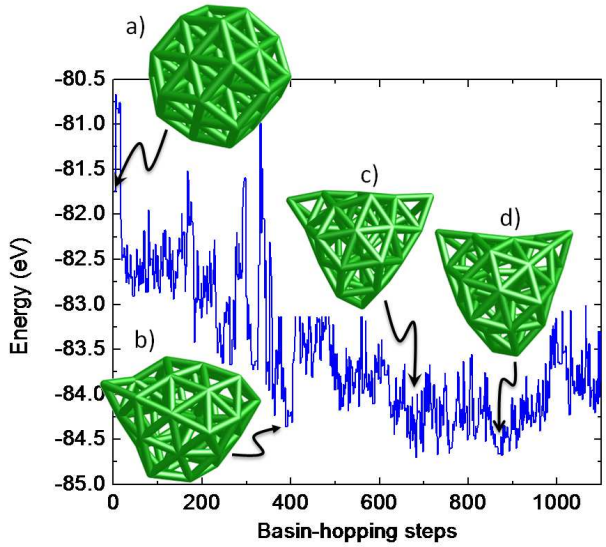

FIG. 1. (Color online) Energy landscape of a DFT-based basin-hopping search for the global minimum of Au_{38}, started with the octahedral structure.

Puzzled by the metallic nature of Au_{38} of the state-of-the-art models and expecting a high-symmetry structure for Au_{40}, we set out to find the global minima of Au_{38} and Au_{40}, hypothesizing that Au_{40}'s structure will build upon that of Au_{38}. Instead of using the empirical potentials to search for global minima before DFT optimization, as previously done for Au_{38} and Au_{40}, we use DFT geometry optimization at the GGA-PBE level[25] directly in our basin-hopping global-minimum search[26]. This approach has been quite powerful for exploring the energy landscape of nanoclusters[27,28]. What distinguishes our work from previous DFT-based basin-hopping search for the similar-sized gold clusters is that we run the basin-hopping procedure for much more steps (over 1000) to explore the energy landscape.

Fig. 1 shows our DFT-based basin-hopping search for the global minimum of Au_{38}, started with the highly symmetric octahedral structure. One can see that the octahedral structure (Fig. 1a) was transformed into much less symmetric configurations of lower energy. The energy lowering is quite substantial, more than 2 eV, instead of the 0.3 to 0.6 eV lowering found by Garzón et al. for their C_s model[22,23]. After a local minimum with one adatom sticking out (Fig. 1b), we found two putative global minima (Fig. 1c and 1d) which are almost degenerate in energy (within 30 meV). The two structures have a similar construction: an Au_4 core and an Au_{32} shell, with two Au adatoms sticking out; but one with C_1 symmetry (Fig. 1c), the other with C_2 symmetry (Fig. 1d). What is unique about the two structures is that they both have a sizable HOMO-LUMO gap, indicating their molecule-like stability in the gas phase. The C_1 structure has a gap of 0.66 eV and the C_2 structure 0.84 eV, unlike the metallic nature of the octahedral structure and Garzón et al.'s C_s model[22,23]. Hence we confirmed that the nanometer-sized Au_{38} still behaves as a molecule.

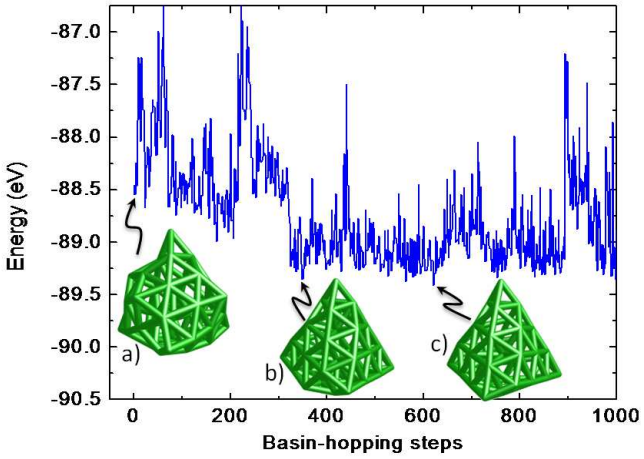

FIG. 2. (Color online) Energy landscape of a DFT-based basin-hopping search for the global minimum of Au_{40}.

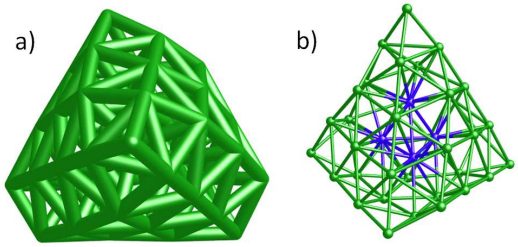

FIG. 3. (Color online) The global minimum for Au_{40} featuring a twisted pyramid with a missing corner: (a) top view, the missing corner is at the top of the figure; (b) side view, the Au_4 tetrahedral core is highlighted.

The two Au_{38} minima are also interesting in that they have two adatoms on the Au_4@Au_{32} core shell. This construction shares some similarity with the Au_{35} structure where one adatom is on the Au_4@Au_{30} core shell[21]. What Au_{38}'s structure suggested to us is that Au_{40}'s structure can build upon the Au_4@Au_{32} core-shell framework but with four adatoms placed in tetrahedral symmetry. This idea led us to propose an initial guess for Au_{40} (Fig. 2a) with two more adatoms manually added to one of the Au_{38}'s two candidate structures (Fig. 1c). Started with this initial guess, we performed DFT-based basin-hopping search for over 1000 steps. Interestingly, twisted pyramid structures evolved out. The first one evolved out is a twisted trigonal pyramid with a missing corner (Fig. 2b and Fig. 3); the core is still an Au_4 tetrahedron (Fig. 3b); overall, the cluster has C_1 symmetry. The second one evolved out is a twisted trigonal pyramid with a missing core atom (Fig. 2c and Fig. 4); this struc-

ture has C_3 symmetry, with an Au_3 triangle core (Fig. 4b). The C_3 symmetry can also be clearly seen from the base of the pyramid (Fig. 4c). The top three layers of the pyramid share the same substructure as the famous tetrahedral Au_{20}. Both Au_{40} structures are chiral as was first proposed for Au_{34}[20].

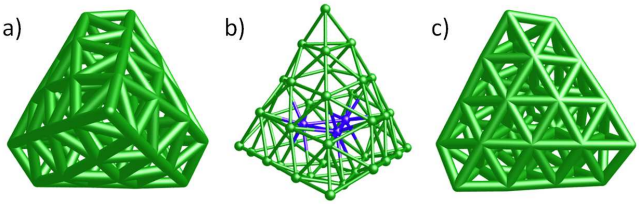

FIG. 4. (Color online) An isomer of Au_{40} featuring a twisted pyramid with C_3 symmetry: (a) top view; (b) side view, showing the Au_3 triangle core; (c) bottom view, showing the base of the pyramid.

To gain a deeper insight into the consequences of the tetrahedral symmetry we now discuss the electronic structure and energetics of the two Au_{40} isomers. We found that the C_1 isomer is the most stable among all the configurations explored; it has a HOMO-LUMO gap of 0.69 eV. The C_3 isomer is only 0.15 eV higher in energy and has an even larger gap of 0.85 eV. So both isomers are stable molecules in nature, given these rather large gaps in clusters of this size. Moreover, we found that if one manually moves the apex atom of the C_1 isomer to the missing corner (Fig. 3a), the resultant structure is only slightly higher in energy (by 0.07 eV), indicating the robustness of Au_{40}'s tetrahedral shape despite the multiple isomers close in energy.

The large HOMO-LUMO gaps of Au_{40} are related to tetrahedral symmetry. In perfectly spherical clusters one finds each DFT Kohn-Sham orbital to be in an unique angular momentum eigenstate relative to the cluster's center of mass. Due to the deformation of the nuclear background away from spherical symmetry these states are not clean anymore. A tetrahedral deformation as present here can be described by an effective potential of the form[12,29]

$$V(\mathbf{r}) = V(r)\left[1 + \alpha_{32}(T_{3,+2} - T_{3,-2})\right] \qquad (1)$$

where $r = |\mathbf{r}|$, the $T_{3,\pm 2}$ are spherical tensor operators and α_{32} is a constant describing the degree of the deformation. The exact form of the $T_{3,\pm 2}$ is not important for our purpose; one only has to note that these operators couple angular momentum eigenstates with angular momentum projections that differ by ± 2 exclusively.

With these considerations we analyze the electronic structure of the tetrahedral gold clusters in Fig. 5[30]. We project the DFT Kohn-Sham orbitals onto spherical angular momentum eigenstates relative to the cluster center of mass to extract their delocalized nature[10]. The usual nomenclature characterizing the states' angular momentum is similar to atomic physics $S, P, D, \ldots$,

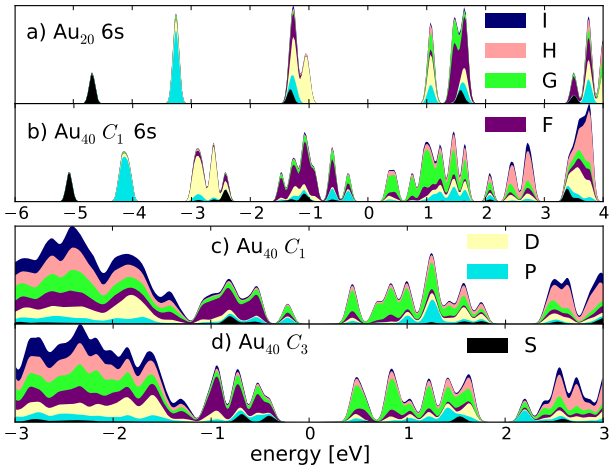

FIG. 5. (Color online) The density of states relative to Fermi energy projected on angular momentum eigenfunctions relative to the clusters center of mass. In a, b) only the Au(6s) electrons are treated as valence electrons, whereas in c, d) also the Au(5d) electrons are allowed to rearrange.

where capital letters distinguish from atom centered angular momenta. The principle quantum number n gives the energetic ordering which is connected to the $(n-1)$ number of radial nodes of the corresponding eigenfunctions. In spherical clusters one would expect the delocalized states to fill $1S^2 1P^6 1D^{10} 2S^2$ orbitals for 20 electrons and additionally the $1F^{14} 2P^6$ orbitals for 40 electrons.

To obtain a clean picture of delocalized states we first fix all the electrons except the Au(6s) electrons in a frozen core approximation. The projected density of states (PDOS) for Au_{20} obtained in this way is presented in Fig. 5a. The states of lowest energy are the delocalized 1S and three 1P states, similar as in the spherical case. This is understandable as the magnetic quantum number of these states is 0, ± 1 and hence these could only couple to higher angular momentum states far away in energy through the $T_{3,\pm 2}$ operators in eq. (1). Then there follows a block of 4 states with mixed S/P/D/F symmetry due to the $T_{3,\pm 2}$ coupling, immediately followed by two states of pure D symmetry that form the Au_{20} HOMO. After the substantial gap of 2.06 eV, the Au_{20} LUMO consists of 3 states with S/P/G symmetry and is followed by a block of 3+2 states of dominant F symmetry. After these there is another large gap. This analysis clearly shows how sparse the delocalized electronic states are distributed under tetrahedral deformations and that the electronic system can make gain from closing shells in the corresponding symmetry.

Analyzing the Au_{40} states in the same way leads to a very comparable picture as shown in Fig. 5b. The relative gaps between the blocks of states gets smaller due to the larger size of the cluster, but the symmetry of the states is similar. In this cluster the rather large HOMO-LUMO gap is between the F/P symmetry dominated oc-

cupied states and the G symmetry dominated unoccupied states. Including Au($5d$) states as valence electrons into the calculation does not change the picture of the frontier orbitals around the Fermi energy as shown in Fig. 5c and d. A comparison with the C_3 isomer that has a clearer tetrahedral structure indicates that in terms of symmetry the HOMO of the C_1 isomer belongs rather to the LUMO block of states with dominant P/G symmetry. As a consequence the gap of the C_3 isomer is even larger than that of the C_1 isomer. Finally we have analyzed the deformation of the s-valence electron density as it was done for the near tetrahedral shape of Na_{40}[31]. While we obtain for the largest distortion parameter $S_3 = 0.04$ for Na_{40}[32] in agreement with ref. 31, $S_3 = 0.26, 0.33$ for the C_1, C_3 isomers of Au_{40} respectively, accounting for the much larger tetrahedral distortion present in the gold clusters.

In summary, we found Au_{40} to be a magic cluster with a quasi-tetrahedral symmetry. It has a twisted pyramid structure discovered from DFT-based basin hopping for global minimum search and built upon the putative global minima of Au_{38}. This cluster is a manifestation of the enhanced stability due to the tetrahedral symmetry, predicted both in nuclear structure and by the jellium model. Analysis of the delocalized electrons in Au_{40} confirms the shell-closing picture by the tetrahedral symmetry, similar to that of Au_{20}. The delocalized $6s$ electrons and the complex energy landscape for clusters such as Au_{40} cannot be accurately described by empirical potentials, thereby making DFT-based global-minimum search a necessity.

This work was supported by the Division of Chemical Sciences, Geosciences, and Biosciences, Office of Basic Energy Sciences, U.S. Department of Energy. This research used resources of the National Energy Research Scientific Computing Center, which is supported by the Office of Science of the U.S. Department of Energy under Contract No. DE-AC02-05CH11231. M.W. acknowledges computational resources from RZ Jülich and the local bwGrid, and funding from Deutsche Forschungsgemeinschaft. We thank M. Moseler for providing the structure of Na_{40}.

[1] H. Häkkinen, M. Moseler, and U. Landman, Phys. Rev. Lett. **89**, 033401 (2002).
[2] H. Häkkinen, Chem. Soc. Rev. **37**, 1847 (2008).
[3] L. Ferrighi, B. Hammer, and G. K. H. Madsen, J. Am. Chem. Soc. **131**, 10605 (2009).
[4] B. Yoon, H. Häkkinen, U. Landman, A. S. Wörz, J.-M. Antonietti, S. Abbet, K. Judai, and U. Heiz, Science **307**, 403 (2005).
[5] J. Li, X. Li, H.-J. Zhai, and L.-S. Wang, Science **299**, 864 (2003).
[6] P. Gruene, D. M. Rayner, B. Redlich, A. F. G. van der Meer, J. T. Lyon, G. Meijer, and A. Fielicke, Science **321**, 674 (2008).
[7] H.-F. Zhang, M. Stender, R. Zhang, C. Wang, J. Li, and L.-S. Wang, J. Phys. Chem. B **108**, 12259 (2004).
[8] B. Yoon, P. Koskinen, B. Huber, O. Kostko, B. von Issendorff, H. Häkkinen, M. Moseler, and U. Landman, Chem. Phys. Chem. **8**, 157 (2007).
[9] W. A. de Heer, Rev. Mod. Phys. **65**, 611 (1993).
[10] M. Walter, J. Akola, O. Lopez-Acevedo, P. D. Jadzinsky, G. Calero, C. J. Ackerson, R. L. Whetten, H. Grönbeck, and H. Häkkinen, Proc. Nat. Acad. Sc. **105**, 9157 (2008).
[11] M. Walter, M. Moseler, R. Whetten, and H. Häkkinen, Chem. Science **2**, 1583 (2011).
[12] I. Hamamoto, B. Mottelson, H. Xie, and X. Zhang, Z. Phys. D **21**, 163 (1991).
[13] J. Dudek, A. Gozdz, N. Schunck, and M. Miskiewicz, Phys. Rev. Lett. **88**, 252502 (2002).
[14] R. A. Bark, J. F. Sharpey-Schafer, S. M. Maliage, T. E. Madiba, F. S. Komati, E. A. Lawrie, J. J. Lawrie, R. Lindsay, P. Maine, S. M. Mullins, S. H. T. Murray, N. J. Ncapayi, T. M. Ramashidza, F. D. Smit, and P. Vymers, Phys. Rev. Lett. **104**, 022501 (2010).
[15] M. Jentschel, W. Urban, J. Krempel, D. Tonev, J. Dudek, D. Curien, B. Lauss, G. de Angelis, and P. Petkov, Phys. Rev. Lett. **104**, 222502 (2010).
[16] Also tetrahedral $[Os_{10}C(CO)_{24}]^{2-}$[33] and $[Os_{20}(CO)_{40}]^{2-}$[34] exist. Their stability is not related to electronic shell closings as indicated by their magnetism[33].
[17] S. M. Reimann, M. Koskinen, H. Häkkinen, P. E. Lindelof, and M. Manninen, Phys. Rev. B **56**, 12147 (1997).
[18] M. Ji, X. Gu, X. Li, X. Gong, J. Li, and L.-S. Wang, Angew. Chem. Int. Ed. **44**, 7119 (2005).
[19] A. F. Jalbout, F. F. Contreras-Torres, L. A. Perez, and I. L. Garzón, J. Phys. Chem. A **112**, 353 (2008).
[20] A. Lechtken, D. Schooss, J. R. Stairs, M. N. Blom, F. Furche, N. Morgner, O. Kostko, B. von Issendorff, and M. M. Kappes, Angew. Chem. Int. Ed. **46**, 2944 (2007).
[21] N. Shao, W. Huang, Y. Gao, L.-M. Wang, X. Li, L.-S. Wang, and X. C. Zeng, J. Am. Chem. Soc. **132**, 6596 (2010).
[22] I. L. Garzón, K. Michaelian, M. R. Beltrán, A. Posada-Amarillas, P. Ordejón, E. Artacho, D. Sánchez-Portal, and J. M. Soler, Phys. Rev. Lett. **81**, 1600 (1998).
[23] I. L. Garzón, M. R. Beltrán, G. González, I. Gutíerrez-González, K. Michaelian, J. Reyes-Nava, and J. I. Rodríguez-Hernández, Eur. Phys. J. D **24**, 105 (2003).
[24] D. T. Tran and R. L. Johnston, Proc. R. Soc. A **467**, 2004 (2011).
[25] Generalized gradient approximation (GGA) as devised by Perdew, Burke and Ernzerhof[35]. Calculations using a higher level meta-GGA approximation[36] yield similar results.
[26] A Python script was used to interface the basin-hopping algorithm[37] and the Vienna Ab initio Simulation Package[38,39] for planewave DFT calculations with the scalar-relativistic projector-augmented wave (PAW) potential for Au which allows use of a low cutoff energy of 172.5 eV. The neutral cluster was placed in the center of a $1.8 \times 1.8 \times 1.8$ nm^3 box. At each step, a full geometry optimization was performed, and the final energy was compared with the previous one for a Metroplis sampling

with a temperature of 7500 K. Then, all Cartesian coordinates were displaced by a random number in [-1,1] times the step size of 0.07 nm. After about 1000 steps which takes 256 parallel cores on a Cray XE6 supercomputer 67 hours to finish, the chosen candidate structures were then finely relaxed with a molecular quantumn chemistry code, Turbomole[40] with the def2-TZVP basis sets.

[27] D. E. Jiang, M. Walter, and S. Dai, Chem. Euro. J **16**, 4999 (2010).

[28] Y. Pei, N. Shao, H. Li, D. E. Jiang, and X. C. Zeng, ACS Nano **5**, 1441 (2011).

[29] N. Schunck, J. Dudek, A. Góźdź, and P. H. Regan, Phys. Rev. C **69**, 061305(R) (2004).

[30] The GPAW package[41,42] performing the PAW method on real space grids with 0.02 nm grid spacing was used for this purpose.

[31] A. Rytkönen, H. Häkkinen, and M. Manninen, Phys. Rev. Lett. **80**, 3940 (1998).

[32] B. Huber, M. Moseler, O. Kostko, and B. v.Issendorff, Phys. Rev. B **80**, 235425 (2009).

[33] D. C. Johnson, R. E. Benfield, P. P. Edwards, W. J. H. Nelson, and M. D. Vargas, Nature **314**, 231 (1985).

[34] A. J. Amoroso, L. H. Gade, B. F. G. Johnson, J. Lewis, P. R. Raithby, and W.-T. Wong, Angew. Chem. Int. Ed. Engl. **30**, 107 (1991).

[35] J. P. Perdew, K. Burke, and M. Ernzerhof, Phys. Rev. Lett. **77**, 3865 (1996).

[36] J. Tao, J. P. Perdew, V. N. Staroverov, and G. E. Scuseria, Phys. Rev. Lett. **91**, 146401 (2003).

[37] D. J. Wales and J. P. K. Doye, J. Phys. Chem. A **101**, 5111 (1997).

[38] G. Kresse and J. Furthmüller, Phys. Rev. B **54**, 11169 (1996).

[39] G. Kresse and J. Furthmüller, Comput. Mater. Sci. **6**, 15 (1996).

[40] R. Ahlrichs, M. Bar, M. Haser, H. Horn, and C. Kolmel, Chem. Phys. Lett. **162**, 165 (1989).

[41] J. J. Mortensen, L. B. Hansen, and K. W. Jacobsen, Phys. Rev. B **71**, 035109 (2005).

[42] J Enkovaara *et al.*, J. Phys. Cond. Mat. **22**, 253202 (2010).